Composites Science and Technology 150 (2017) 181–186

Contents lists available at ScienceDirect

Composites Science and Technology

journal homepage: http://www.elsevier.com/locate/compscitech

# Numerical predictions of fiber orientation and mechanical properties for injection-molded long-glass-fiber thermoplastic composites

Huan-Chang Tseng*, Rong-Yeu Chang, Chia-Hsiang Hsu

*CoreTech System (Moldex3D) Co., Ltd., ChuPei City, Hsinchu County, 30265, Taiwan*

ARTICLE INFO

*Article history:*
Received 7 April 2017
Accepted 25 July 2017
Available online 27 July 2017

*Keywords:*
Long-glass-fiber-reinforced thermoplastic composites
Shell-core orientation structure
Fiber orientation prediction
Mechanical properties
Injection molding simulation

ABSTRACT

Achieving accurate numerical predictions of the orientation of fiber in a shell-core structure is a critical requirement for improving mechanical performance and carrying out structural analysis for long fiber-reinforced thermoplastics (LFRT) in injection molding. When using 3D-mesh computation, the orientation in the shell layer was predicted fairly well, but resulted in over-predictive deviation in relation to the core region. Recently, an objective orientation model, iARD-RPR (improved ARD model and Retarding Principal Rate model), was developed in the rheological field of fiber suspension. We therefore used the iARD-RPR model to enhance the prior fiber orientation predictions in 3D injection molding simulation. For various LFRT composites with the same concentration (40 wt%) of glass fiber immersed in two different polymer matrices (polypropylene and polyamide 6,6), the mechanical properties depending on fiber orientation are estimated to a significant degree, and their reinforced performance further compared.



## 1. Introduction

Long fiber-reinforced thermoplastic (LFRT) composites have been applied in the automotive industry due to their great potential; in fact, these materials offer much better mechanical performance than the short-fiber composites. Anisotropic fiber orientation of shell-core structure strongly influences the reinforced ability of a final LFRT product. Developing process models and computational tools to predict the microstructure of these composites is important for actual practice.

In the past years, the Pacific Northwest National Laboratory (PNNL) and the Oak Ridge National Laboratory (ORNL) have actively integrated the predictive engineering tools for injection-molded fiber composites, including glass fiber and carbon fiber [1–3]. Accurate predictions of fiber orientation are available for an ultimate mechanical/structural analysis. Tucker and coworkers (University of Illinois) [4,5] developed the primary fiber orientation model with six parameters, ARD-RSC (Anisotropic Rotary Diffusion and Reduced Strain Closure). This model has been implemented in commercial injection molding simulation software [1–3], ASMI (Autodesk Simulation Moldflow Insight). Nguyen et al. used the ASMI midplane-mesh computation, which was based on the Hele-Shaw approximation [6], and obtained validation of the ARD-RSC model's orientation predictions through their excellent agreement with actual experimental results for various long glass fiber composites. However, generating a midplane mesh for a complex 3D geometric part is a very time-consuming task that lacks numerical resolution.

Unfortunately, the ARD-RSC model employed in ASMI 3D-mesh computation has produced unsatisfactory/inaccurate predictions of fiber orientation. While the results indicated that the orientation in the shell layer was predicted fairly well, over-prediction deviation was found in regard to the core region. The need to resolve this issue is an industrial imperative. Recently, Tseng et al. [7–9] further studied the classic fiber orientation models in seeking to develop a new objective model, iARD-RPR (Improved Anisotropic Rotary Diffusion and Retarding Principal Rate). They were successful and the model has since been incorporated into the commercial software of 3D injection molding simulation, Moldex3D. It is significant that the iARD-RPR computation requires just three parameters, and does not require an inlet condition set near the gate. For short-glass-fiber orientation predictions, Foss et al. [10] demonstrated that the use of one set of the optimal iARD-RPR parameters was able to yield good orientation predictions with respect to flow factors, such as fill rate and part geometry.

So far, only a few attempts have been made to probe the

* Corresponding author.
*E-mail address:* ivortseng@moldex3d.com (H.-C. Tseng).

http://dx.doi.org/10.1016/j.compscitech.2017.07.026
0266-3538/

inaccurate 3D predictions of long fiber orientation for the previous PNNL-ORNL project. An effective method for improving the ARD-RSC model in 3D apparently was not sought. In the present study, we therefore used the iARD-RPR model to enhance the long fiber orientation computation in the 3D injection molding simulation. These predicted shell-core orientation distributions were compared to the PNNL-ORNL experimental data and the previous ARD-RSC results. In addition, the predicted fiber orientation was provided to estimate the mechanical properties and discuss the reinforced performance of the fiber composites.

## 2. Theoretical background

A *single* fiber is regarded as a rigid cylindrical rod. The fiber's unit vector **p** along its axis direction can describe the fiber orientation. For a concise representation of the orientation of a large population of fibers, Advani and Tucker [11] defined the second order orientation tensor as:

$$\mathbf{A} = \oint \psi(\mathbf{p})\mathbf{pp}d\mathbf{p} = \begin{bmatrix} A_{11} & A_{12} & A_{13} \\ A_{12} & A_{22} & A_{23} \\ A_{13} & A_{23} & A_{33} \end{bmatrix} \tag{1}$$

where $\psi(\mathbf{p})$ is the probability density distribution function over the orientation space; **A** is the symmetric matrix and its trace is $A11+A22+A33 = 1$. Physically, $\mathbf{A} = \mathbf{I}/3$ represents the isotropic orientation state, wherein **I** is the identity matrix. Three diagonal components: *A11*, *A22* and *A33*, correspond to the flow, cross-flow and thickness directions, respectively.

$\mathbf{A}_4$ is the fourth order orientation tensor and is symmetric, defined as:

$$\mathbf{A}_4 \oint \psi(\mathbf{p})\mathbf{pppp}d\mathbf{p}. \tag{2}$$

The $\mathbf{A}_4$ calculation decoupled in terms of **A** is obtained by higher order polynomial closure approximations, such as the Eigenvalue-Based Optimal Fitting (EBOF) Closure [12,13], the Invariant-Based Optimal Fitting (IBOF) Closure [14], and the neural network-based closure [15]. It is known that the validity of the closure approximations depends on flow type and fiber orientation. Note that the accuracy of IBOF is as good as EBOF, and IBOF requires less computational time to obtain a solution [14].

A time-evolution equation of the second-order orientation tensor is fixed on the material derivative, denoted as $\dot{\mathbf{A}}$. Over the last three decades, theoretical researchers in the fiber suspension rheological field have made considerable effort to determine the dynamic fiber orientation states. The classic Folgar-Tucker model is famous to predict short fiber orientation. The modern orientation models include the Phelps-Tucker ARD (Anisotropic Rotary Diffusion) model [5], the Wang-Tucker RSC (Reduced Strain Closure) model [4] and the ARD-RSC model [5]. These models are adopted available in commercial injection molding simulation software, the Autodesk Simulation Moldflow Insight (ASMI). Following these models, Tseng et al. [7–9] further developed a new objective fiber orientation model, namely, iARD-RPR (improved ARD model and Retarding Principal Rate model) with just three parameters. Here we introduce both the ARD-RSC and the iARD-RPR models.

### 2.1. ARD-RSC model with six-parameter

Phelps and Tucker [5] constructed the ARD model, while they coupled it with the RSC model of Wang et al. [4]. This combinative model is called as ARD-RSC, as below:

$$\begin{aligned} \dot{\mathbf{A}}^{\text{ARD-RSC}} = {} & \mathbf{W}\cdot\mathbf{A} - \mathbf{A}\cdot\mathbf{W} + \xi\{\mathbf{D}\cdot\mathbf{A} + \mathbf{A}\cdot\mathbf{D} - 2[\mathbf{A}_4 + (1-\kappa)(\mathbf{L}_4 \\ & - \mathbf{M}_4 \\ & : \mathbf{A}_4)] : \mathbf{D}\} + \dot{\gamma}\{2[\mathbf{D}_r - (1-\kappa)\mathbf{M}_4 \\ & : \mathbf{D}_r] - 2\kappa\text{tr}(\mathbf{D}_r)\mathbf{A} - 5(\mathbf{D}_r\cdot\mathbf{A} + \mathbf{A}\cdot\mathbf{D}_r) + 10[\mathbf{A}_4 \\ & + (1-\kappa)(\mathbf{L}_4 - \mathbf{M}_4 \\ & : \mathbf{A}_4)] : \mathbf{D}_r\} \end{aligned} \tag{3}$$

$$\xi = \frac{a_r^2 - 1}{a_r^2 + 1} \tag{4}$$

$$\mathbf{L}_4 = \sum_{i-1}^{3} \lambda_i \mathbf{e}_i\mathbf{e}_i\mathbf{e}_i\mathbf{e}_i \tag{5}$$

$$\mathbf{M}_4 = \sum_{i-1}^{3} \mathbf{e}_i\mathbf{e}_i\mathbf{e}_i\mathbf{e}_i \tag{6}$$

$$\mathbf{D}_r = b_1\mathbf{I} + b_2\mathbf{A} + b_3\mathbf{A}^2 + \frac{b_4}{\dot{\gamma}}\mathbf{D} + \frac{b_5}{\dot{\gamma}^2}\mathbf{D}^2 \tag{7}$$

where **W** is the vorticity tensor; **D** is the rate-of-deformation tensor; $\dot{\gamma}$ is the shear rate of **D**, $\dot{\gamma} = \sqrt{2\mathbf{D} : \mathbf{D}}$; $\xi$ is the particle shape factor; and $a_r$ is the fiber aspect ratio. Note that two particular fourth orientation tensors, $\mathbf{M}_4$ and $\mathbf{L}_4$, are related to eigenvalues $\lambda_i$ and eigenvectors $\mathbf{e}_i$ of **A**. Since $a_r >> 1$, $\xi$ is assumed to signify unity. The factor $\kappa$ is constrained between 0 and 1, and is generally in a range between 0.05 and 0.2 [4] in dimensionless units. When $\kappa = 1$, the RSC equation can recover to the Folgar-Tucker equation. Details of the RSC model are available elsewhere [4], and are not repeated here.

The ARD-RSC model contains a set of six material parameters which can be identified using a target orientation state. In principle, the target orientation state is chosen in which the injection filling flow in an edge-gated plaque is representative of a steady, simple shear flow; and therefore, the identification procedure uses the average fiber orientation components in the shell layers near the gate region to determine the ARD-RSC parameters. A valid set of parameters $b_i$ must satisfy the criteria proposed by Phelps and Tucker [5].

In order to enhance the predictive accuracy of the fiber orientation in the RSC and ARD-RSC computations, an inlet condition of fiber orientation distribution is necessitated to be set around a gate area. The inlet condition involves the user-defined mode (if possessing experimental data) and the specified mode (artificially, to define aligned orientation at the skin and transverse/random orientation at the core). Nguyen et al. [16] pointed out that the inlet condition strongly influences the orientation predictions of the RSC the ARD-RSC models. Those orientation predictions [16–19] achieved by the midplane-mesh and 3D-mesh simulations were in good agreement with experimental data.

### 2.2. iARD-RPR model with three-parameter

Based on the previous orientation models, Tseng et al. [7–9] developed a new model, the iARD-RPR. However, the iARD tensor does not pass the classic rheological rule of Euclidean objectivity, namely, material frame indifference. It is hard to ignore the non-objective effect due to the fact that different coordinate systems

can yield different answers. More recently, Tseng et al. [9] have improved such a non-objective issue and then proposed the objective iARD model. Here, we introduce the objective iARD-RPR model divided into three parts.

First, the iARD-RPR equation contains three terms: the Jeffery Hydrodynamics (HD) $\dot{\mathbf{A}}^{\mathrm{HD}}$, the iARD $\dot{\mathbf{A}}^{\mathrm{iARD}}$, and the RPR $\dot{\mathbf{A}}^{\mathrm{RPR}}$, presented as:

$$\dot{\mathbf{A}} = \dot{\mathbf{A}}^{\mathrm{HD}} + \dot{\mathbf{A}}^{\mathrm{iARD}}(C_I, C_M) + \dot{\mathbf{A}}^{\mathrm{RPR}}(\alpha) \tag{8}$$

$$\dot{\mathbf{A}}^{\mathrm{HD}} = (\mathbf{W}\cdot\mathbf{A} - \mathbf{A}\cdot\mathbf{W}) + \xi(\mathbf{D}\cdot\mathbf{A} + \mathbf{A}\cdot\mathbf{D} - 2\mathbf{A}_4 : \mathbf{D}) \tag{9}$$

where $\dot{\mathbf{A}}^{\mathrm{iARD}}$ has two available parameters: the fiber-fiber interaction parameter $C_I$ and the fiber-matrix interaction parameter $C_M$; $\dot{\mathbf{A}}^{\mathrm{RPR}}$ has one parameter $\alpha$, which is meant to slow down the response rate of the fiber orientation.

Second, it is significant that the rotary diffusion tensor $\mathbf{D}_r$ depends on the square of the objective rate-of-deformation tensor for defining a new iARD model [9], as below:

$$\dot{\mathbf{A}}^{\mathrm{iARD}} = \dot{\gamma}[2\mathbf{D}_r - 2\mathrm{tr}(\mathbf{D}_r)\mathbf{A} - 5\mathbf{D}_r\cdot\mathbf{A} - 5\mathbf{A}\cdot\mathbf{D}_r + 10\mathbf{A}_4 : \mathbf{D}_r] \tag{10}$$

$$\mathbf{D}_r = C_I\left(\mathbf{I} - C_M\frac{\mathbf{D}^2}{\|\mathbf{D}^2\|}\right) \tag{11}$$

where $\mathbf{D}$ is the symmetric part of the velocity-gradient tensor $\mathbf{L}$, $\mathbf{D} = \frac{1}{2}(\mathbf{L}^{\mathrm{T}} + \mathbf{L})$. The scalar $\|\mathbf{D}^2\| = \sqrt{\frac{1}{2}\mathbf{D}^2 : \mathbf{D}^2}$ is the norm of tensor $\mathbf{D}^2$.

Lastly, the RPR model is introduced as:

$$\dot{\mathbf{A}}^{\mathrm{RPR}} = -\mathbf{R}\cdot\dot{\mathbf{\Lambda}}^{\mathrm{IOK}}\cdot\mathbf{R}^{\mathrm{T}} \tag{12}$$

$$\dot{\Lambda}_{ii}^{\mathrm{IOK}} = \alpha\dot{\lambda}_i, \quad i,j,k = 1,2,3 \tag{13}$$

where $\dot{\mathbf{\Lambda}}^{\mathrm{IOK}}$ is the material derivative of a particular diagonal tensor and its superscript indicates the intrinsic orientation kinetics (IOK) assumption [7,8]; $\mathbf{R}$ is the rotation matrix and $\mathbf{R}^{\mathrm{T}}$ is the transpose of $\mathbf{R}$; the superscript T is the transpose operator of a matrix throughout this paper; $\lambda_i$ is the eigenvalues of $\mathbf{A}$, $\lambda_1 \geq \lambda_2 \geq \lambda_3$; and $\mathbf{R} = [\mathbf{e}_1, \mathbf{e}_2, \mathbf{e}_3]$ is defined by eigenvector columns of $\mathbf{A}$.

The iARD-RPR model has only the three physical parameters: a fiber-fiber interaction parameter $C_I$, a fiber-matrix interaction parameter $C_M$ and a slow-down parameter $\alpha$. The available region of these three parameters is suggested in: $0 < C_I < 0.1$, $0 < C_M < 1$, $0 < \alpha < 1$. In addition, the shell-orientation layer depends on the iARD parameters, while the core width is controlled by the RPR parameter.

The iARD-RPR model has been implemented in the commercial injection molding simulation software, Moldex3D (CoreTech System Co. of Taiwan), to allow for the fiber orientation predictions. Accordingly, the accurate predictions of the fiber orientation model are contingent on the method and assumptions of the underlying numerical modeling during the injection mold filling. Besides, the initial condition of the fiber orientation tensor at the runner entrance was set as the isotropic state. An experimental inlet condition did not need to be set around a gate, due to the higher 3D numerical resolution and the solid runner system consideration in computation.

## 3. Results and discussion

Based on the disclosed reports of the 2012 U.S. PNNL-ORNL project [1], two materials used were 40 wt% long glass fiber (LGF)-reinforced polypropylene (PP) and polyamide 6,6 (PA66) composites, abbreviated as 40 wt%LGF/PP and 40 wt%LGF/PA66, respectively. The geometry of injection molding is a center-gated plaque, as illustrated in Fig. 1. The flow direction is towards to X-axis; the cross-flow Z-axis; the thickness direction Y-axis. The plaque dimensions were 600 mm × 600 mm × 3 mm. There is one measurement point located on a center line 140 mm from the injection location of the center-gated plaques. The processing conditions, including filling time, mold temperature, and melting temperature for different materials are addressed in Table 1.

The 3-D model was first developed with one of the CAD (Computer Aided Design) programs, and then meshed by creating hexagonal (HEXA) elements with 21 layers, as shown in Fig. 1. In this study, the Moldex3D simulation program (R15) was used in the plaque during the injection molding process. All the material parameters, including the PVT, shear viscosity, specific heat, and thermal conductivity, are available elsewhere [20].

The viscosity flow curve is always of concern in suspension rheology. Fig. 2 shows the shear viscosity against the shear rate at a temperature of 300 °C for two different composites. The viscosity curves are described by the Yield-Cross-WLF model [27]. For the generalized Newtonian fluids of polymer melts, a typical flow curve involves the Newtonian plateau at low shear rates, and shear thinning at high shear rates. In particular regard to the long fiber composites, the power-law viscosity is obviously found at low shear rates, namely the low-shear-rate shear thinning viscosity, also called the yield-stress viscosity [21–24].

### 3.1. Fiber orientation prediction with experimental validation

The related experimental orientation data and the validated ARD-RSC results were referred to in previous PNNL project reports [1]. All of the fiber orientation predictions were performed in the 3D injection molding simulations via ASMI (Autodesk Simulation Moldflow Insight). Six ARD-RSC parameters for the 40 wt%LGF/PP and 40 wt%LGF/PA66 composites are addressed in Table 2.

In the present work, we adopted the iARD-RRP model implemented in the Moldex3D to enable fiber orientation predictions in the 3D injection molding simulation of the end-gated plaque (see

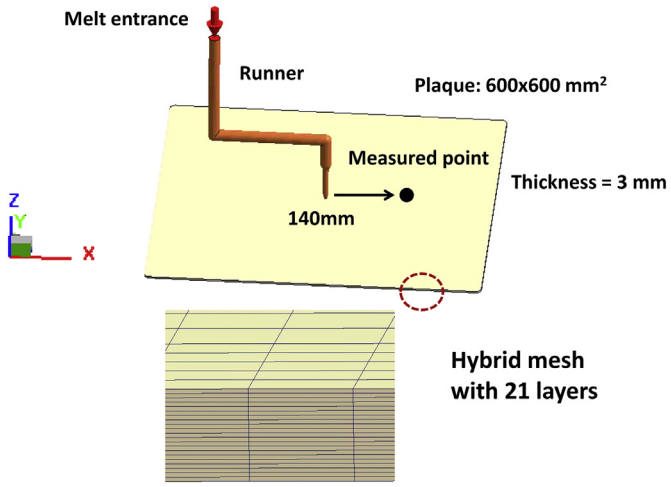


**Fig. 1.** Illustration of injection molded geometry for the center-gated plaque with one measured region.

**Table 1**
Injection molding conditions for various long fiber reinforced thermoplastic composites.

| | 40 wt% LGF/PP | 40 wt% LGF/PA66 |
|---|---|---|
| Injection time (sec) | 5.35 | 4.56 |
| Mold temperatures (°C) | 38 | 100 |
| Melting temperatures (°C) | 266 | 310 |

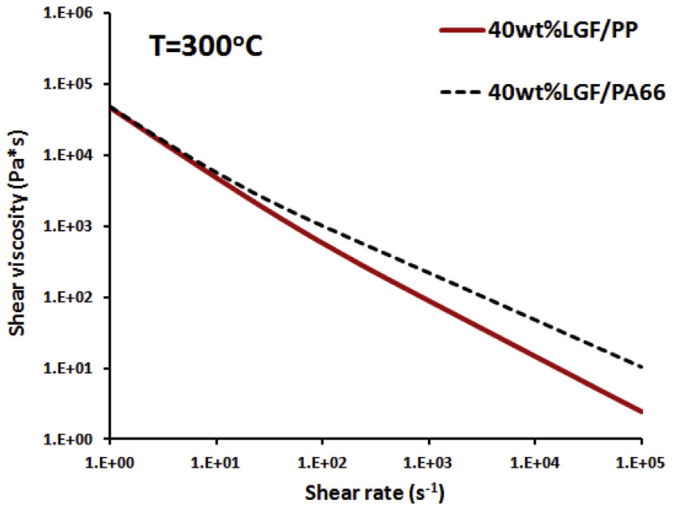


**Fig. 2.** Viscosity flow curve of the Yield-Cross-WLF model for various fiber composites, 40 wt%LGF/PP and 40 wt%LGF/PA66.

**Table 2**
Six parameters of the ARD-RSC model for various long fiber reinforced thermoplastic composites.

| | 40 wt% LGF/PP | 40 wt% LGF/PA66 |
|---|---|---|
| $b_1$ | $1.006 \times 10^{-4}$ | $1.762 \times 10^{-4}$ |
| $b_2$ | $3.232 \times 10^{-3}$ | $1.504 \times 10^{-3}$ |
| $b_3$ | $4.000 \times 10^{-3}$ | $7.000 \times 10^{-3}$ |
| $b_4$ | $1.671 \times 10^{-3}$ | $2.073 \times 10^{-4}$ |
| $b_5$ | $2.500 \times 10^{-4}$ | 0 |
| $\kappa$ | 0.25 | 0.1 |

**Table 3**
Three parameters of the iARD-RPR model for various long fiber reinforced thermoplastic composites.

| | 40 wt% LGF/PP | 40 wt% LGF/PA66 |
|---|---|---|
| $C_I$ | 0.0005 | 0.0005 |
| $C_M$ | 0.5 | 0.7 |
| $\alpha$ | 0.1 | 0.1 |

Fig. 1). The iARD-RRP parameters used are given in Table 3. Figs. 3 and 4 show the predicted gap-wise distribution of fiber orientation tensor components at the measured point of the plaque for the 40 wt%LGF/PP and 40 wt%LGF/PA66 composites, respectively. Note that $A_{11}$ and $A_{22}$ are defined as the flow-direction ($X$-axis) and the cross-flow-direction ($Z$-axis) orientation tensor components. Fibers in the shell layers were more aligned with the flow direction, characterized by the large values of $A_{11}$ and the low values of $A_{22}$; conversely, the core layer was quite wide, with low values of $A_{11}$ and high values of $A_{22}$, representing a cross-flow orientation state. In the shell layer, the fibers were oriented near the walls in the flow direction by the shear deformations, which were maximal; the

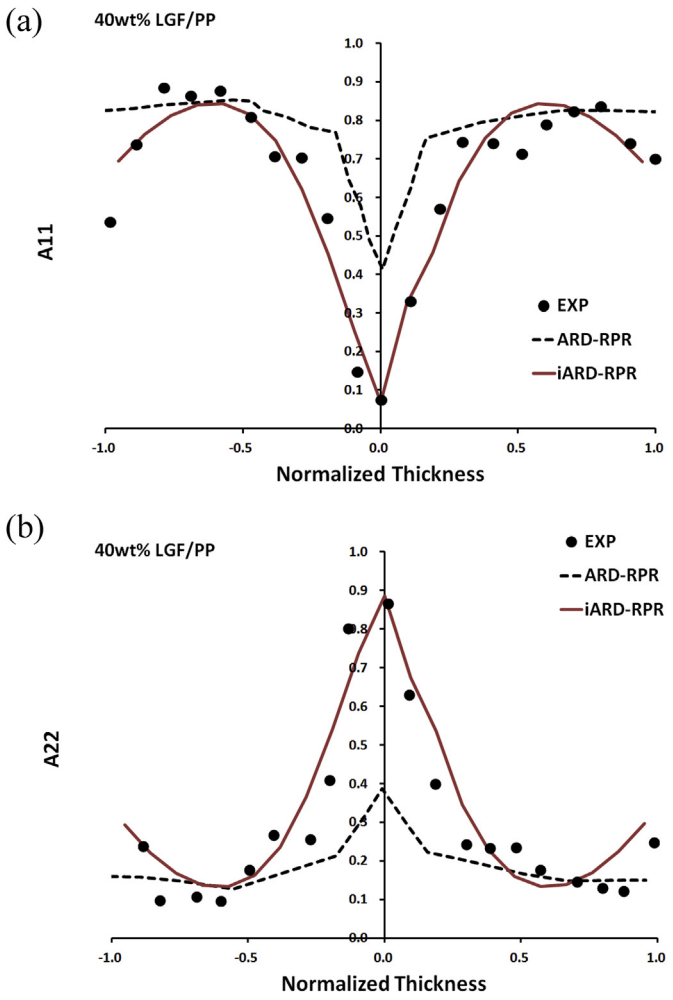


**Fig. 3.** Comparison between experimental data and model predictions of orientation components, (a) $A_{11}$ and (b) $A_{22}$, through the normalized thickness for 40 wt%LGF/PP. Note that the dash and solid lines indicates the ARD-RSC model and the iARD-RPR model, respectively.

others were oriented in the core, wherein the deformations were weak. As shown in the figures, the fiber orientation distributions exhibited a shell–core–shell structure according to the experimental points (see the symbols).

As a whole, the iARD-RPR predictions for the core region and shell layers agree fairly well with the PNNL-ORNL results in the fiber orientation data. However, the previous ARD-RSC results in 3D-ASMI could only capture the shell layers correctly; they provided inaccurate over-predictions of the core region. In addition, the orientation distribution is slightly asymmetrical [1]. The iARD-RPR computation *just needs three parameters*, and does not require an inlet condition set near the gate. However, it appears as though lacking any criteria governing those ARD-RSC parameters (see Table 1) with respect to two different matrices under the same fiber concentration is inconvenient. For this reason, *excess parameters* may cause numerical instability or non-physical behaviors in the computing process if the parameters are not carefully adjusted [5]. Hence, a default parameter set is always used. van Haag et al. [25] performed an automated optimization procedure to obtain a material-specific set of the ARD-RSC parameters, thereby providing substantial help for researchers. Correspondingly, the iARD-RPR parameters could be flexibly set with respect to various fiber composites.

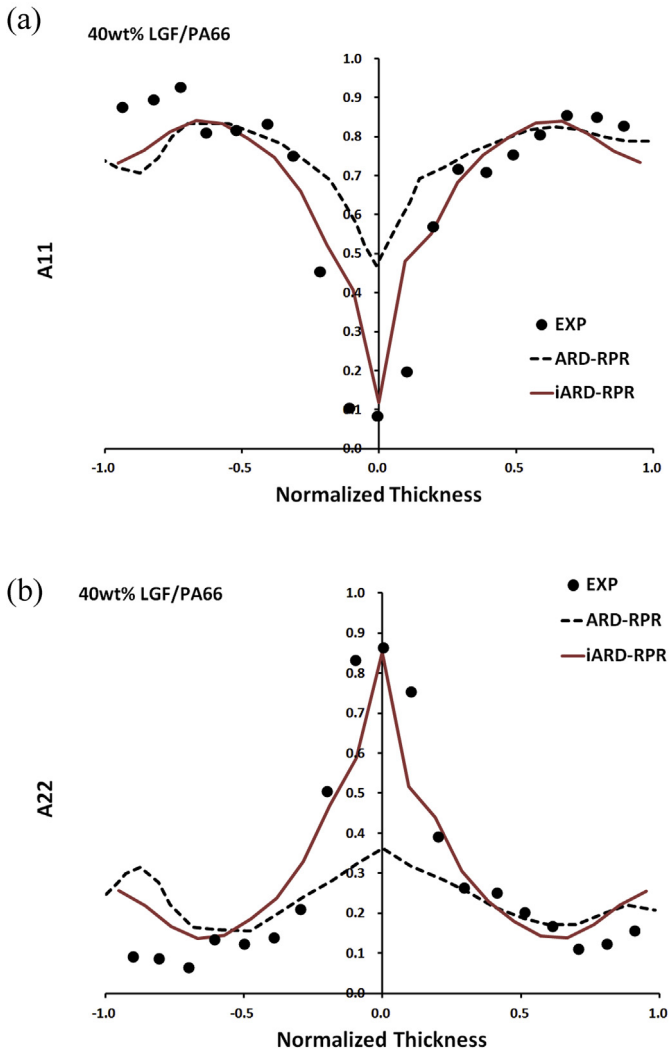


**Fig. 4.** Comparison between experimental data and model predictions of orientation components, (a) $A_{11}$ and (b) $A_{22}$, through the normalized thickness for 40 wt%LGF/PA66. Note that the dash and solid lines indicates the ARD-RSC model and the iARD-RPR model, respectively.

On the other hand, the inlet boundary condition is necessitated in the RSC and ARD-RSC computation for effectively improving the accuracy of the fiber orientation predictions. Previously, Nguyen et al. [16] pointed out that the inlet condition strongly influences the orientation predictions of the RSC in the ARD-RSC models. Those optimal parameters possibly interfered with the artificial or experimental inlet condition. In our 3D computation, the initial condition of the fiber orientation tensor at the runner entrance is set as the isotropic state. Using the inlet condition is unnecessary for iARD-RPR, due to the higher 3D numerical resolution and the solid runner system consideration in the computation.

### 3.2. Mechanical property analysis of reinforced ability

A micromechanical material modeling software, Digimat-MF, based on the Mori-Tanaka Mean Field homogenization scheme [26], was used to compute the mechanical performance of the fiber-reinforced thermoplastic composites. In the foregoing section, we generated these fiber orientation predictions, validated with the disclosed experimental data on the injection-molded long carbon fiber thermoplastic composites. Thus, in regard to the primary objective, discussing the effect of fiber orientation on mechanical properties, the predicted orientation data resulting from using iARD-RPR were integrated into the Digimat-MF computation.

**Table 4**
Micro-mechanical properties of pure PP and PA66 matrix resins.

| | PP | PA66 |
|---|---|---|
| Resin density (g/cm$^3$) | 0.92 | 1.14 |
| Resin modulus (GPa) | 1.45 | 3.75 |
| Resin Poissons ratio | 0.4 | 0.35 |

**Table 5**
Micro-mechanical properties of glass fibers.

| | Value |
|---|---|
| Fiber density (g/cm$^3$) | 2.54 |
| Fiber diameter (μm) | 14 |
| Fiber weight fraction | 0.4 |
| Fiber modulus (GPa) | 72 |
| Fiber Poissons ratio | 0.22 |

For the Digimat-MF, the material properties of the pure PP and PA66 matrix resins are summarized in Table 4, while those of the glass fiber are listed in Table 5. According to the previous PNNL report [1], the weight-average fiber length $L_w$ is given in Table 6. From the fiber orientation distribution in the last section, the thickness-averaged values, $<A_{11}>$ and $<A_{22}>$, are included in Table 6 for the 40 wt%LGF/PP and 40 wt%LGF/PA66 composites. Based on these data, we applied Digimat-MF to obtain the maximum tensile modulus $E_1$: about 7.3 GPa for the 40 wt%LGF/PP, and 11.4 GPa for the 40 wt%LGF/PA66. Here, the experimental modulus $E_{exp}$ is taken from web page of both the PlastiComp and Dupont Technical Data Sheets: 7.5 GPa and 11.5 GPa. The predicted modulus is very close to the experimental data. Such an integration of the primary fiber orientation computation to estimate mechanical properties is dependable.

We further made a comparison of pure matrix and composites for the modulus. By adding the same fiber concentration of 40 wt% LGFs, the reinforcing performance of modulus increment $\Delta E$ for the PA66 composite (~8 GPa) is more effective than the PP composite (~6 GPa), as shown in Fig. 5. The stress against strain in various fiber composites is presented in Fig. 6. The same as the modulus $E_1$ results above, it is evident that the stress-strain response obtained 40 wt%LGF/PA66 > 40 wt%LGF/PP. This finding is related to the modulus. Overall, adding a large amount of long glass fibers to pure PA66 is more effective in enhancing mechanical performance than to pure PP.

## 4. Conclusions

We have demonstrated that using the iARD-RPR model to calculate fiber orientation can obtain accurate predictions of the

**Table 6**
Weight-averaged fiber length $L_w$, aspect ratio $a_r$, thickness-averaged orientation tensor components $<A_{11}>$ and $<A_{22}>$, and tensile modulus $E_1$ at the center of the center-gated plaque for various materials with the experimental bulk value of tensile modulus $E_{exp}$.

| | $L_w$ (mm) | $a_r$ | $<A_{11}>$ | $<A_{22}>$ | $E_1$ (GPa) | $E_{exp}$ (GPa) |
|---|---|---|---|---|---|---|
| 40 wt% LGF/PP | 1.71[a] | 122 | 0.659 | 0.323 | 7.262 | 7.586[b] |
| 40 wt% LGF/PA66 | 1.10[a] | 78 | 0.689 | 0.294 | 11.492 | 11.500[c] |

[a] Taken from Ref. [1].
[b] Taken from Web Page of Dupont Technical Data Sheet.
[c] Taken from Web Page of PlastiComp Technical Data Sheet.

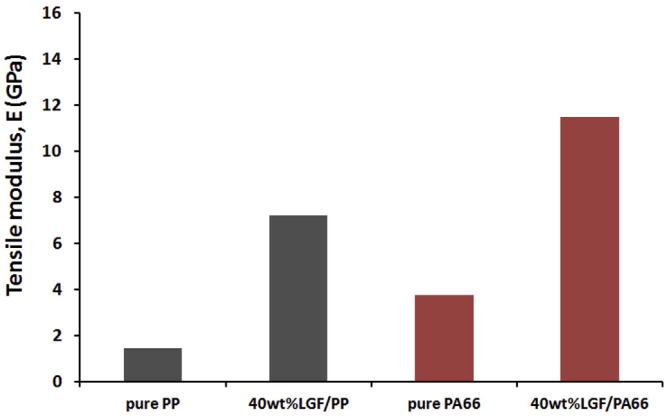


**Fig. 5.** Bar char of the predictive tensile modulus against various fiber composites with experimental data of pure PP and pure PA66.

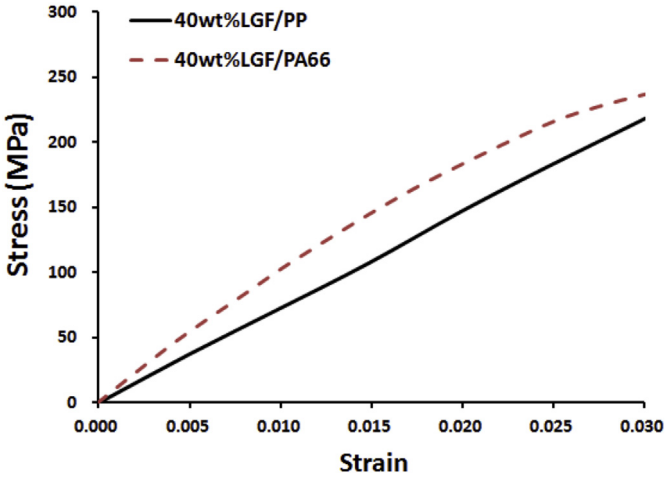


**Fig. 6.** Stress against strain responses for various fiber composites, (a) 40 wt% LGF/PP and (b) 40 wt% LGF/PA66.

well-known shell-core structure. More importantly, such a model *just needs three parameters*, and needs no inlet condition set near the gate. In addition, the fiber orientation predictions are provided to estimate the tensile modulus, which are in good agreement with the experimental data. Thus, the integration of fiber orientation and mechanical property is dependable in carrying out structural analysis. As a result, adding a large amount of long glass fibers to pure PA66 is more effective in enhancing mechanical performance than to pure PP. In future work, we will focus on the complex geometry of designing high-quality parts, involving various changes in the direction of the flow, the inclusion of ribs and the changes in the thickness and holes. This will be challenging for an integration simulation.

## References

[1] N. Nguyen, X. Jin, J. Wang, V. Kunc, C.L. Tucker III, Validation of New Process Models for Large Injection-molded Long-fiber Thermoplastic Composite Structures, PNNL Report under Contract DE-AC05–76RL01830, The US Department of Energy, Pacific Northwest National Laboratory, 2012. PNNL-21165.

[2] N. Nguyen, X. Jin, J. Wang, J.H. Phelps, C.L. Tucker III, V. Kunc, S.K. Bapanapalli, M.T. Smith, Implementation of New Process Models for Tailored Polymer Composite Structures into Processing Software Packages, PNNL Report under Contract DE-AC05–76RL01830, The US Department of Energy, Pacific Northwest National Laboratory, 2010. PNNL-19185.

[3] J. Wang, P. Cook, A. Bakharev, F. Costa, D. Astbury, Prediction of fiber orientation in injection-molded parts using three-dimensional simulations, in: AIP Conference Proceedings, vol. 1713, 2016, p. 040007.

[4] J. Wang, J.F. O'Gara, C.L. Tucker III, An objective model for slow orientation kinetics in concentrated fiber suspensions: theory and rheological evidence, J. Rheol. 52 (2008) 1179–1200.

[5] J.H. Phelps, C.L. Tucker III, An anisotropic rotary diffusion model for fiber orientation in short- and long-fiber thermoplastics, J. Newt. Fluid Mech. 156 (2009) 165–176.

[6] P. Kennedy, R. Zheng, Flow Analysis of Injection Molds, Hanser Publishers, Munich, Germany, 2013.

[7] H.-C. Tseng, R.-Y. Chang, C.-H. Hsu, Method and Computer Readable Media for Determining Orientation of Fibers in a Fluid, 2013. US Patent (8,571,828).

[8] H.-C. Tseng, R.-Y. Chang, C.-H. Hsu, Phenomenological improvements to predictive models of fiber orientation in concentrated suspensions, J. Rheol. 57 (2013) 1597–1631.

[9] H.-C. Tseng, R.-Y. Chang, C.-H. Hsu, An objective tensor to predict anisotropic fiber orientation in concentrated suspensions, J. Rheol. 60 (2016) 215–224.

[10] P.H. Foss, H.-C. Tseng, J. Snawerdt, Y.-J. Chang, W.-H. Yang, C.-H. Hsu, Prediction of fiber orientation distribution in injection molded parts using moldex3d simulation, Polym. Compos 35 (2014) 671–680.

[11] S.G. Advani, C.L. Tucker III, The use of tensors to describe and predict fiber orientation in short fiber composites, J. Rheol. 31 (1987) 751–784.

[12] J.S. Cintra Jr., C.L. Tucker III, Orthotropic closure approximations for flow-induced fiber orientation, J. Rheol. 39 (1995) 1095–1122.

[13] B.E. VerWeyst, Numerical Predictions of Flow-induced Fiber Orientation in Three-dimensional Geometries, Ph.D. Thesis, University of Illinois at Urbana-Champaign, 1998.

[14] D.H. Chung, T.H. Kwon, Invariant-based optimal fitting closure approximation for the numerical prediction of flow-induced fiber orientation, J. Rheol. 46 (2002) 169–194.

[15] D.A. Jack, B. Schache, D.E. Smith, Neural network-based closure for modeling short-fiber suspensions, Polym. Compos 31 (2010) 1125–1141.

[16] B.N. Nguyen, L.S. Fifield, S.A. Kijewski, M.D. Sangid, J. Wang, F. Costa, C.L. Tucker III, R.N. Mathur, U.N. Gandhi, S. Mori, Predictive Engineering Tools for Injection-molded Long-carbon-fiber Thermoplastic Composites, FY 2015 Second Quarterly Report, The US Department of Energy, Pacific Northwest National Laboratory, 2015. PNNL-24259 (PNNL Report under Contract DE-AC05–76RL01830).

[17] B.N. Nguyen, L.S. Fifield, R.N. Mathur, S.A. Kijewski, M.D. Sangid, J. Wang, X. Jin, F. Costa, U.N. Gandhi, S. Mori, Charles L. Tucker III, Predictive Engineering Tools for Injection-molded Long-carbon-fiber Thermoplastic Composites - Fy 2014 Fourth Quarterly Report, PNNL Report under Contract DE-AC05–76RL01830, The US Department of Energy, Pacific Northwest National Laboratory, 2014. PNNL-23842.

[18] B.N. Nguyen, L.S. Fifield, A. Yocum, C. Schutte, Predictive Engineering Tools for Injection-molded Long-carbon-fiber Thermoplastic Composites, FY 2014 Annual Progress Report-Lightweight Materials, Pacific Northwest National Laboratory (PNNL), the US Department of Energy, 2014, pp. 192–205.

[19] J. Wang, B.N. Nguyen, R. Mathur, B. Sharma, M.D. Sangid, F. Costa, X. Jin, C.L. Tucker III, L.S. Fifield, Fiber orientation in injection molded long carbon fiber thermoplastic composites, in: SPE ANTEC Conference, 2015. Technical Papers.

[20] Moldex3D, User Manual and Material Database, CoreTech System, Hsinchu, Taiwan, 2017.

[21] H.M. Laun, Orientation effects and rheology of short glass fiber-reinforced thermoplastics, Colloid Polym. Sci. 262 (1984) 257–269.

[22] S.G. Advani, Flow and Rheology in Polymer Composites Manufacturing, Elsevier, New York, 1994.

[23] S. Han, K.K. Wang, C.A. Hieber, Characterization of the rheological properties of a fast-curing epoxy-molding compound, J. Rheol. 41 (1997) 177–195.

[24] J. Richeton, S. Ahzi, K.S. Vecchio, F.C. Jiang, R.R. Adharapurapu, Influence of temperature and strain rate on the mechanical behavior of three amorphous polymers: characterization and modeling of the compressive yield stress, Int. J. Solids Struct. 43 (2006) 2318–2335.

[25] J. van Haag, C. Bontenackels, C. Hopmann, Fiber orientation prediction of long Fiber-reinforced thermoplastics: Optimization of model parameters, in: SPE ANTEC Conference, 2015. Technical Papers.

[26] T.D. Papathanasiou, D.C. Guell, Flow-induced Alignment in Composite Materials, Woodhead, Cambridge, 1997.

[27] H.-C. Tseng, R.-Y. Chang, C.-H. Hsu, Improved fiber orientation predictions for injection molded fiber composites, Compos. Appl. Sci. Manuf. 99 (2017) 65–75.